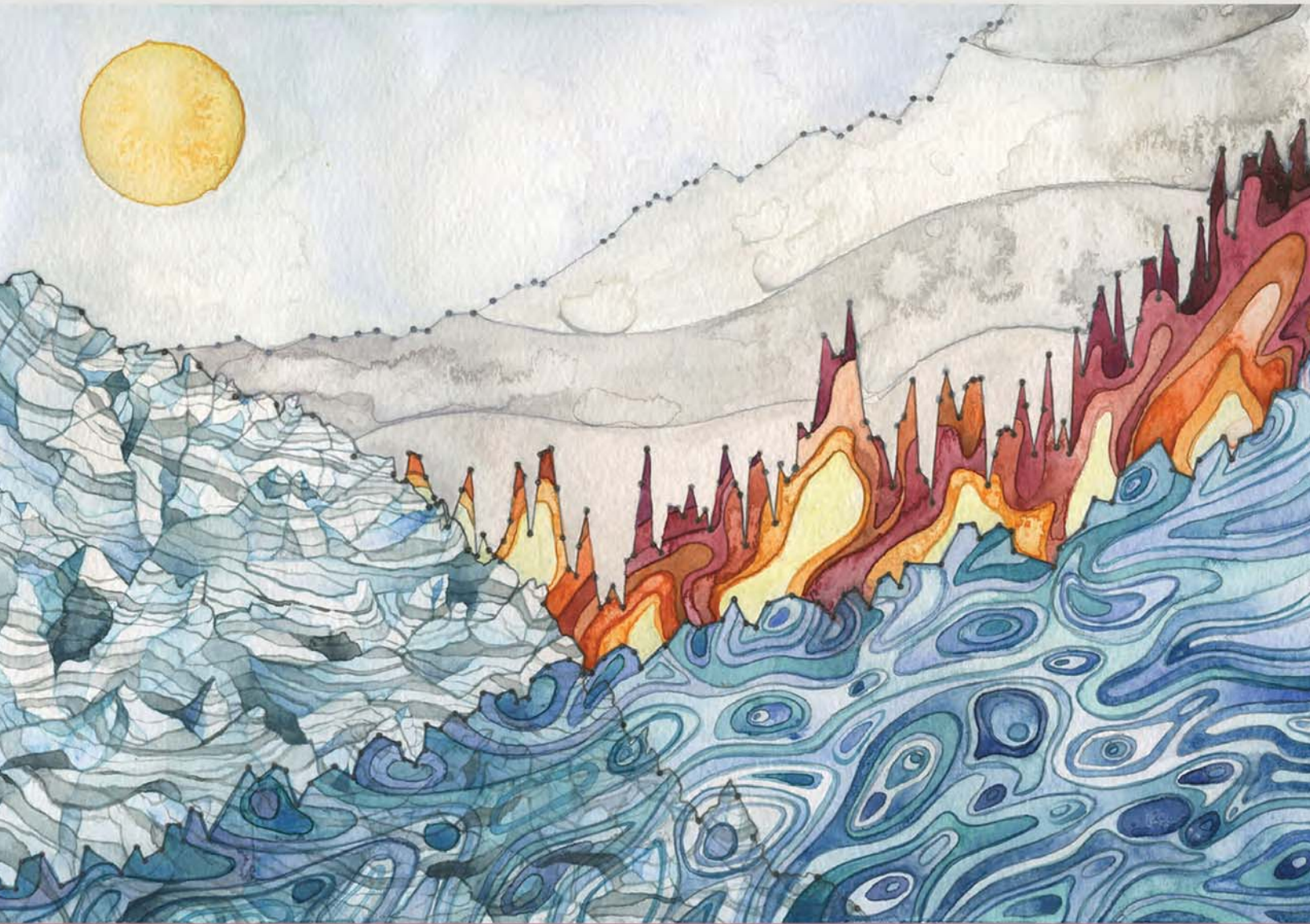


STATE OF THE CLIMATE IN 2015



Special Supplement to the
Bulletin of the American Meteorological Society
Vol. 97, No. 8, August 2016

speeds of 116 kt (60 m s^{-1}) on 3 August. Its high translation speed ($\sim 5\text{--}8 \text{ m s}^{-1}$) during intensification helped to reduce the ocean cooling during the TC life cycle, thus supplying more air–sea flux for intensification (Lin et al. 2009). This was the most intense storm to strike Saipan, CNMI, in the last 25 years. Cooling of the surface waters of over 5°C was observed under the full track of this typhoon, while cooling of the upper ocean layers (TCHP) was restricted to between 135° and 150°E .

- Hurricane Patricia (Fig. 4.38d) was the most intense tropical cyclone ever recorded in the Western Hemisphere in terms of barometric pressure, and the strongest ever recorded globally in terms of maximum sustained winds of 185 kt (95 m s^{-1} ; Kimberlain et al. 2016). Patricia started as a tropical depression off the coast of Mexico on 20 October, and developed into a Category 5 storm within 66 hours. During its rapid intensification the TCHP values were higher than 80 kJ cm^{-2} .
- Hurricane Joaquin (Fig. 4.38e) was an intense TC that evolved near the Bahamas on 26 September and was one of the strongest storms to affect these islands. Joaquin underwent rapid intensification and became a Category 3 hurricane on 1 October, exhibiting maximum sustained winds of approximately 135 kt (69 m s^{-1}) on 3 October (Berg 2016). The upper ocean conditions were supportive of Atlantic tropical cyclone intensification (Maineli et al. 2008). This rapid intensification occurred during a short travel time over very high TCHP values ($> 100 \text{ kJ cm}^{-2}$). The cooling of the ocean waters was evident both in the upper layer and at the surface.

g. Atlantic warm pool—C. Wang

The description and characteristics of the Atlantic warm pool (AWP), including its multidecadal variability, have been previously described (e.g., Wang 2015). Figure 4.39 shows the extension of the AWP time series through 2015 varying on different time scales.

While the AWP in 2015 showed similarities to 2014, there were some key differences. As in 2014, the AWP in 2015 was larger than its climatological mean each month, with the largest AWP occurring in September (Fig. 4.40a). However, the AWP in 2015 started in February and lasted through December, longer than its normal period of May to October, and had an anomalously larger value in November. After starting in February, the AWP appeared in the Gulf of Mexico in June (Fig. 4.40b). By July and August, the AWP was well developed in the Gulf of Mexico and Caribbean Sea and reached eastward into the western

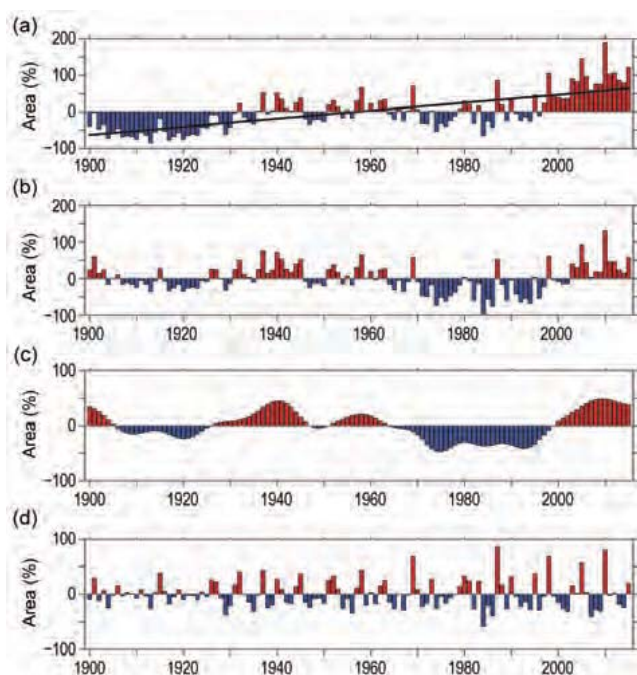


FIG. 4.39. The AWP index for 1900–2015. The AWP area index (%) is calculated as the anomalies of the area of SST warmer than 28.5°C divided by the climatological Jun–Nov AWP area. Shown are the (a) total, (b) detrended (removing the linear trend), (c) multidecadal, and (d) interannual area anomalies. The multidecadal variability is obtained by performing a 7-year running mean to the detrended AWP index. The interannual variability is calculated by subtracting the multidecadal variability from the detrended AWP index. The black straight line in (a) is the linear trend that is fitted to the total area anomaly. The extended reconstructed SST dataset is used.

tropical North Atlantic (Figs. 4.40c,d). By September, the AWP had further expanded southeastward and the 28.5°C isotherm covered nearly the entire tropical North Atlantic (Fig. 4.40e). The AWP started to decay after October when the waters in the Gulf of Mexico began cooling (Fig. 4.40f). In November, the 28.5°C isotherm still covered the Caribbean Sea and part of the western North Atlantic Ocean (Fig. 4.40g).

The effect of the AWP on TC steering flows and tracks has been previously documented (Wang 2015). The TC steering flow anomalies were consistent with those of other observed large AWP years (Wang et al. 2011). The TC steering flow anomalies during the North Atlantic TC season are depicted in Fig. 4.41. With the exception of June and November, the TC steering flow anomalies were unfavorable for TCs making landfall in the United States. From July to October, the TC steering flow anomalies were mostly southward or eastward in the western tropical North Atlantic, and northward and northeastward in the open ocean of the North Atlantic. This distribution

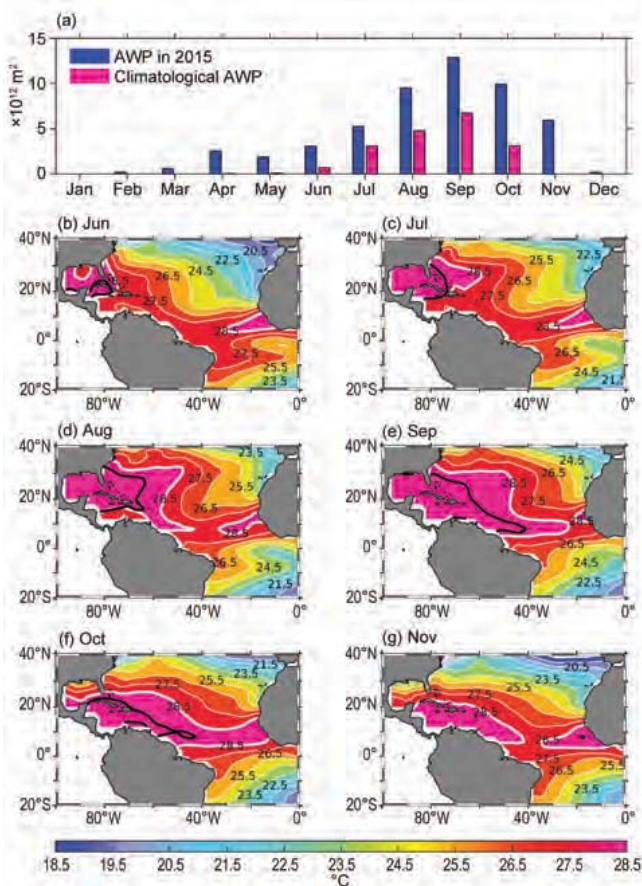


FIG. 4.40. (a) The monthly AWP area in 2015 (10^{12} m²; blue) and the climatological AWP area (red) and the spatial distributions of the 2015 AWP in (b) Jun, (c) Jul, (d) Aug, (e) Sep, (f) Oct, and (g) Nov. The AWP is defined by SST larger than 28.5°C. The black thick contours in (b)–(g) are the climatological AWP based on the data from 1971 to 2000 and the white thick contours are the 2015 28.5°C SST values. The extended reconstructed SST dataset is used.

of these anomalies was consistent with the fact that for all TCs that formed in the Atlantic MDR, none made landfall in the United States. For the two land-falling North Atlantic TCs (Ana and Bill), neither one formed in the Atlantic MDR (see section 4e2).

h. Indian Ocean dipole—J.-J. Luo

Year-to-year climate variability in the tropical Indian Ocean (IO) is largely driven by local ocean-atmosphere interactions and ENSO (e.g., Luo et al. 2010). Among the former, the Indian Ocean dipole (IOD) represents one major internal climate mode in the IO, which may exert significant climate impacts on countries surrounding the IO. The IOD often starts to grow in boreal summer, peaks in September–November, and deteriorates rapidly in December in association with the reversal of monsoonal winds along the west coast of Sumatra. During late boreal summer to fall 2015, a positive IOD occurred for the

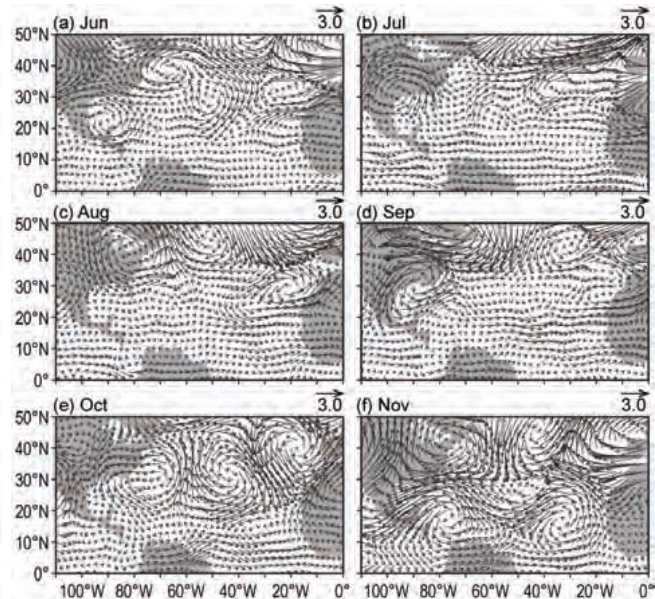


FIG. 4.41. The TC steering flow anomalies (10^3 hPa m s⁻¹) in the 2015 Atlantic TC season of (a) Jun, (b) Jul, (c) Aug, (d) Sep, (e) Oct, and (f) Nov. The TC steering flow anomalies are calculated by the vertically averaged wind anomalies from 850 hPa to 200 hPa relative to the 1971–2000 climatology. The NCEP–NCAR reanalysis field (Kalnay et al. 1996) is used.

first time since the last positive IOD event in 2012 (Luo 2013). The positive IOD in 2015 is the 10th such event since 1981.

SSTs and upper ocean (0–300 m) mean temperature in most of the tropical IO were warmer than normal throughout the year (Figs. 4.42, 4.43), in association with the influence of a strong El Niño in the Pacific and a pronounced long-term warming trend of the IO SST in recent decades (e.g., Luo et al. 2012). During December–February 2014/15, surface westerly anomalies occurred across the equatorial IO, corresponding to the dry–wet contrast between the IO and the Maritime Continent–western Pacific (Figs. 4.42a, 4.43a). This is consistent with a central Pacific–El Niño condition. The westerly anomalies across the equatorial IO shallow (deepen) the oceanic thermocline in the western (eastern) IO, which helps induce cold (warm) SST anomalies in the equatorial western (eastern) IO (Figs. 4.42a, 4.43a). From March to November, in accordance with a rapid development of a strong El Niño in the Pacific (see Fig. 4.3), rainfall over the Indonesia–western Pacific decreased due to a weakened Walker Cell. Meanwhile, SSTs in the western IO increased quickly and reached $\sim 0.8^\circ\text{C}$ greater than the climatology (1982–2014) during September–November (Figs. 4.42, 4.44). Correspondingly, easterly anomalies developed in the IO beginning in boreal spring (Figs. 4.43, 4.44). Weak anomalous southeasterlies initially appeared along the west coast